INSTITUTE OF PHYSICS PUBLISHING JOURNAL OF PHYSICS G: NUCLEAR AND PARTICLE PHYSICS

J. Phys. G: Nucl. Part. Phys. **31** (2005) 1303–1327 doi:10.1088/0954-3899/31/11/013

Shape trends and triaxiality in neutron-rich odd-mass Y and Nb isotopes

Y X Luo[1,2,3], J O Rasmussen[3], I Stefanescu[4], A Gelberg[5], J H Hamilton[1], A V Ramayya[1], J K Hwang[1], S J Zhu[1,6], P M Gore[1], D Fong[1], E F Jones[1], S C Wu[7], I Y Lee[3], T N Ginter[3,8], W C Ma[9], G M Ter-Akopian[10], A V Daniel[10], M A Stoyer[11] and R Donangelo[12]

[1] Physics Department, Vanderbilt University, Nashville, TN 37235, USA
[2] Institute of Modern Physics, Chinese Academy of Sciences, Lanzhou 730000, People's Republic of China
[3] Lawrence Berkeley National Laboratory, Berkeley, CA 94720, USA
[4] KU Leuven, Instituut voor Kern-en Stralingsfysica, Celestijnenlaan 200 D, B-3001 Leuven, Belgium
[5] Institut für Kernphysik, Universität zu Köln, 50937 Köln, Germany
[6] Physics Department, Tsinghua University, Beijing 100084, People's Republic of China
[7] Department of Physics, National Tsing Hua University, Hsinchu, Republic of China
[8] National Superconducting Cyclotron Laboratory, Michigan State University, East Lansing, MI 48824, USA
[9] Department of Physics, Mississippi State University, MS 39762, USA
[10] Flerov Laboratory for Nuclear Reactions, JINR, Dubna, Russia
[11] Lawrence Livermore National Laboratory, Livermore, CA 94550, USA
[12] Universidade Federal do Rio de Janeiro, CP 68528, RG, Brazil

Received 27 May 2005
Published 26 September 2005
Online at stacks.iop.org/JPhysG/31/1303

Abstract

New level schemes of odd-Z ^{99,101}Y ($Z = 39$) and ^{101,105}Nb ($Z = 41$) are established based on the measurement of prompt gamma rays from the fission of ^{252}Cf at Gammasphere. Bands of $\pi 5/2^+[422]$, $\pi 5/2^-[303]$ and $\pi 3/2^-[301]$ are observed and extended to provide spectroscopic information concerning nuclear shapes in this important odd-Z region. In combination with the level structure of the odd-Z Tc ($Z = 43$), Rh ($Z = 45$) and the neighbouring even-Z isotopes the level systematics, signature splittings and kinematic and dynamic moments of inertia of the bands in the Y and Nb isotopes are discussed in terms of shape transition and triaxiality. The pronounced difference observed in the signature splittings between Y and Tc, Rh isotopes is interpreted as evidence of the axially symmetric deformed shape in the Y isotopes, and, as previously reported, large and near maximum triaxiality in Tc–Rh isotopes. The likely lowering of crossing frequencies of the ground-state bands in Tc and Rh isotones in comparison with those in Y isotones also implies a shape transition from axially symmetric deformed shapes in Y nuclei to triaxiality in Tc and Rh isotones. Triaxial-rotor-plus-particle model calculations strongly support a pure axially symmetric shape with large quadrupole deformation in Y isotopes. The model calculations yielded γ values ranging from -19° to

-13° for the $5/2^+[422]$ ground-state bands of ^{101,103,105}Nb and of -5° for the two negative-parity bands in ^{101}Nb. The fact that Nb isotopes have intermediate values of signature splitting and band crossing frequencies between those of Y and Tc, Rh isotopes is interpreted as that the Nb isotopes are transitional nuclei with regard to triaxial deformation. A correlation of quadrupole deformations and of triaxiality is seen in the neutron-rich nuclei with $Z = 39$–45.

1. Introduction

Studies of shape transitions and shape coexistence in neutron-rich nuclei with $A \sim 100$ have long been of major importance [1, 2]. Intensive investigations have been carried out for even–even nuclei in this region. Large quadrupole deformations [3], the onset of superdeformed ground states and identical bands [2, 4, 5], shape evolutions and shape coexistence [4–8] were observed in the Sr ($Z = 38$)–Zr ($Z = 40$)–Mo ($Z = 42$) region. The abrupt shape transitions from spherical to strongly deformed ground states in Sr and Zr isotopes and the smoother change in shape transition in nuclei with $Z > 40$ are attributed to the appearance of triaxiality for $Z > 40$ even-Z nuclei. An early work on triaxial degree of freedom in Mo isotopes was reported in [9]. Recently, differences in band crossing frequencies and signature splittings have been observed in the $\upsilon h_{11/2}$ bands between Zr and Mo isotopes and ascribed to the triaxial degree of freedom in Mo and the mainly axially symmetric shape in Zr isotopes [10], indicating a transition from the axially symmetric shape in Zr ($Z = 40$) to triaxiality in Mo ($Z = 42$) isotopes.

Spectroscopic information of the odd-Z neighbours is of great interest in understanding the shape transitions and the importance of the triaxial degree of freedom in this nuclear region. A shape transition from axially symmetric to triaxial deformation in the odd-Z nuclei of this region is expected and of particular interest. However, less has been reported for the odd-Z neighbours so far. High-spin states in ^{99,101,103}Tc ($Z = 43$, $N = 56$, 58, 60) have been studied and the single-proton states located around the Fermi level were discussed as a function of deformation [11, 12, 13]. Triaxial deformation was observed in ^{105}Rh ($Z = 45$, $N = 60$) and used to explain the large signature splitting in the ground-state band based on a $g_{9/2}$ odd proton, while a shape change from triaxial (in the ground-state band) to prolate deformation (in the three-quasiparticle band with very small signature splitting) was discussed [14]. High-spin structures in ^{107,109,111,113}Rh and ^{105,107,109}Tc were studied and revealed shape coexistence and the role played by triaxiality in these Tc and Rh isotopes [15, 16, 17, 18]. Our GANDS2000 collaboration published detailed results on odd-Z, neutron-rich ^{111,113}Rh ($Z = 45$) [17] isotopes and ^{105,107,109}Tc ($Z = 43$) [18] isotopes. The data yielded new level schemes with the highest excitation energies and spins yet established and considerably expanded weakly populated bands to provide rich spectroscopic information [17, 18]. Triaxial-rotor-plus-particle model calculations performed with $\varepsilon_2 = 0.32$ and $\gamma = -22.5^\circ$ on the prolate side of near maximum triaxiality yielded the best reproduction of the excitation energies, signature splittings and branching ratios of the positive-parity bands (except for the intruder bands) in Tc isotopes [18]. The model calculations gave the best fits to positive-parity bands in Rh isotopes at near maximum triaxiality with $\varepsilon_2 = 0.27$–0.28, $\gamma = -28^\circ$ (see[17]).

In the lower odd-Z region with $Z = 39$–41, where the triaxiality-related shape transition is expected to occur, still less-extended level schemes have been reported because of the comparatively weak populations from fission. Low-lying levels populated by beta decay were reported in [19] and the references therein. The $\pi 5/2^+[422]$, $\pi 5/2^-[303]$ and $\pi 3/2^-[301]$

bands populated in Y and Nb isotopes by fission were proposed. Limited level schemes of ^{99,101}Y were reported [8, 20–23] and those of ^{101,103}Nb were first given in [8, 24]. Well-developed $\pi 5/2^+[422]$ and $\pi 5/2^-[303]$ bands can be found in ^{103}Nb in [25]. No decay data have been reported for ^{105}Nb. The $\pi 5/2^+[422]$ band with only five levels was proposed in ^{105}Nb based on measurements of prompt gamma transitions from the spontaneous fission of ^{248}Cm [8].

We report in this paper new results on neutron-rich Y ($Z = 39$) and Nb ($Z = 41$) isotopes. New level schemes of ^{99}Y ($N = 60$), ^{101}Y ($N = 62$), ^{101}Nb ($N = 60$) and ^{105}Nb ($N = 64$) are proposed. By combining the data and results of the neighbouring even-Z and odd-Z isotopes, signature splittings, kinematic and dynamic moments of inertia as a function of spin and rotational frequencies in the Y and Nb isotopes are discussed in terms of triaxial and quadrupole deformations for the $N = 60$, 62, 64 isotonic chains. Triaxial-rotor-plus-particle model calculations were performed and reproduced the level excitations, signature splittings and branching ratios of the observed bands in Y and Nb isotopes. Shape transitions with regard to triaxiality and correlation of quadrupole deformations and triaxiality are discussed for neutron-rich nuclei in this $Z = 39$–45 region.

2. Experiment and data analysis

Measurements of prompt γ rays from a fission source by using multi-gamma detection arrays have been shown to be a powerful tool for population and detection of high-spin states of neutron-rich nuclei [4]. For two runs each taking 2 weeks in 2000, a ^{252}Cf source of 62 μCi, sandwiched between two 10 mg cm^{-2} Fe foils, was placed in an 8 cm polyethylene ball centred in the Gammasphere [26], which then consisted of 102 Compton-suppressed Ge detectors. The polyethylene ball was used to absorb β rays and conversion electrons, as well as to partially moderate and absorb fission neutrons. Accumulation of over 5.7×10^{11} triple and higher-fold events provided excellent conditions for experimental observations for higher spin states and weakly populated bands.

A Radware cube three-dimensional histogram was created [27] without specifying time-to-amplitude converter timing gates, giving triple-coincidence events with $\sim$1 μs resolving time. To clarify ambiguities caused by peak overlapping, a less-compressed Radware cube was also used. In comparison with the regular Radware cube with its standard for compression of 8192 channels over $\sim$5 MeV one-third less compression was performed to build a less-compressed cube. As we mentioned in [18] for studies of Tc isotopes, the less-compressed cube was found to be useful in clarifications of ambiguities related to peak overlapping, in identifications of weak transitions and bands smeared by contaminating strong transitions in the coincidence spectra and in the least-squares fitting of transition energies with higher precisions. The first observation of the weakly populated and smeared $K = 1/2$ intruder band in ^{105}Tc using the less-compressed cube is a good example of the advantage of using it [18].

By following the methods based on the coincident production of the complementary fission partners described in [17], the triple-coincidence data were analysed to identify new transitions and to establish the new level schemes of ^{99,101}Y and ^{101,105}Nb. Transition energies and relative intensities were determined by using the least-squares peak-fitting of Radford's gf3 program [27]. Figures 1(a)–(f) provide examples of many double-gated, triple-coincidence spectra for analysis of ^{99}Y, ^{101}Y, ^{101}Nb and ^{105}Nb, respectively. For figures 1(a), (b), (d)–(f), with gates on two of the ground-state band transitions in the studied nucleus, coincident transitions of the nucleus studied and those of its known fission partners are seen in these spectra, and so

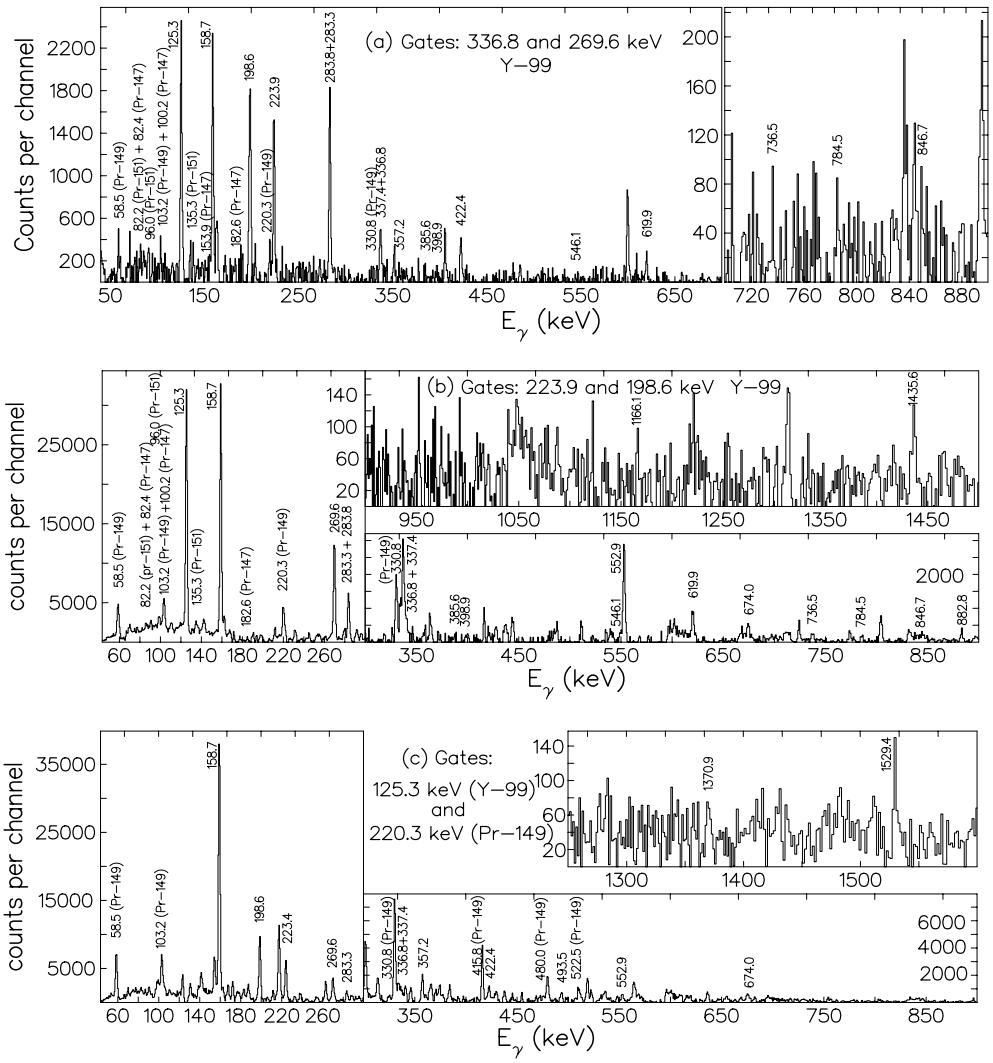

Figure 1. (a) A double-gated, triple-coincidence spectrum for ^{99}Y analysis. Gates were set on the 336.8 keV and 269.6 keV transitions of ^{99}Y. All the coincident transitions of ^{99}Y and its known fission partners' transitions are simultaneously seen in the spectrum. The 736.5 keV, 784.5 keV and 846.7 keV transitions can also be seen in (b). (b) A double-gated, triple-coincidence spectrum for ^{99}Y analysis. Gates were set on the 223.9 keV and 198.6 keV transitions of ^{99}Y. All the coincident transitions of ^{99}Y, including the decay-out transitions of the 2142.1 keV isomer state, and the known fission partners' transitions are simultaneously observed in the spectrum. (c) A double-gated, triple-coincidence spectrum for ^{99}Y analysis, showing the observations of the decay-out transitions of band (4), the 1529.4 keV and 1370.9 keV transitions. Gates were set on the 125.3 keV transition of ^{99}Y and the 220.3 keV transition of its 4*n* fission partner ^{149}Pr. The strong coincident transitions in both ^{99}Y and ^{149}Pr are simultaneously seen in the spectrum. (d) A double-gated, triple-coincidence spectrum for ^{101}Y analysis. Gates were set on the 289.8 keV and 276.4 keV transitions of ^{101}Y. All the coincident transitions of ^{101}Y and those of its known fission partners are simultaneously observed in the spectrum. (e) A double-gated, triple-coincidence spectrum for ^{101}Nb analysis. Gates were set on the 433.3 keV and 119.5 keV transitions of ^{101}Nb. All the coincident transitions of ^{101}Nb and those of its known fission partners are simultaneously observed in the spectrum. (f) A double-gated, triple-coincidence spectrum for ^{105}Nb analysis. Gates were set on the 272.8 keV and 310.9 keV transitions of ^{105}Nb. All the coincident transitions of ^{105}Nb and those of its known fission partners are simultaneously observed in the spectrum.

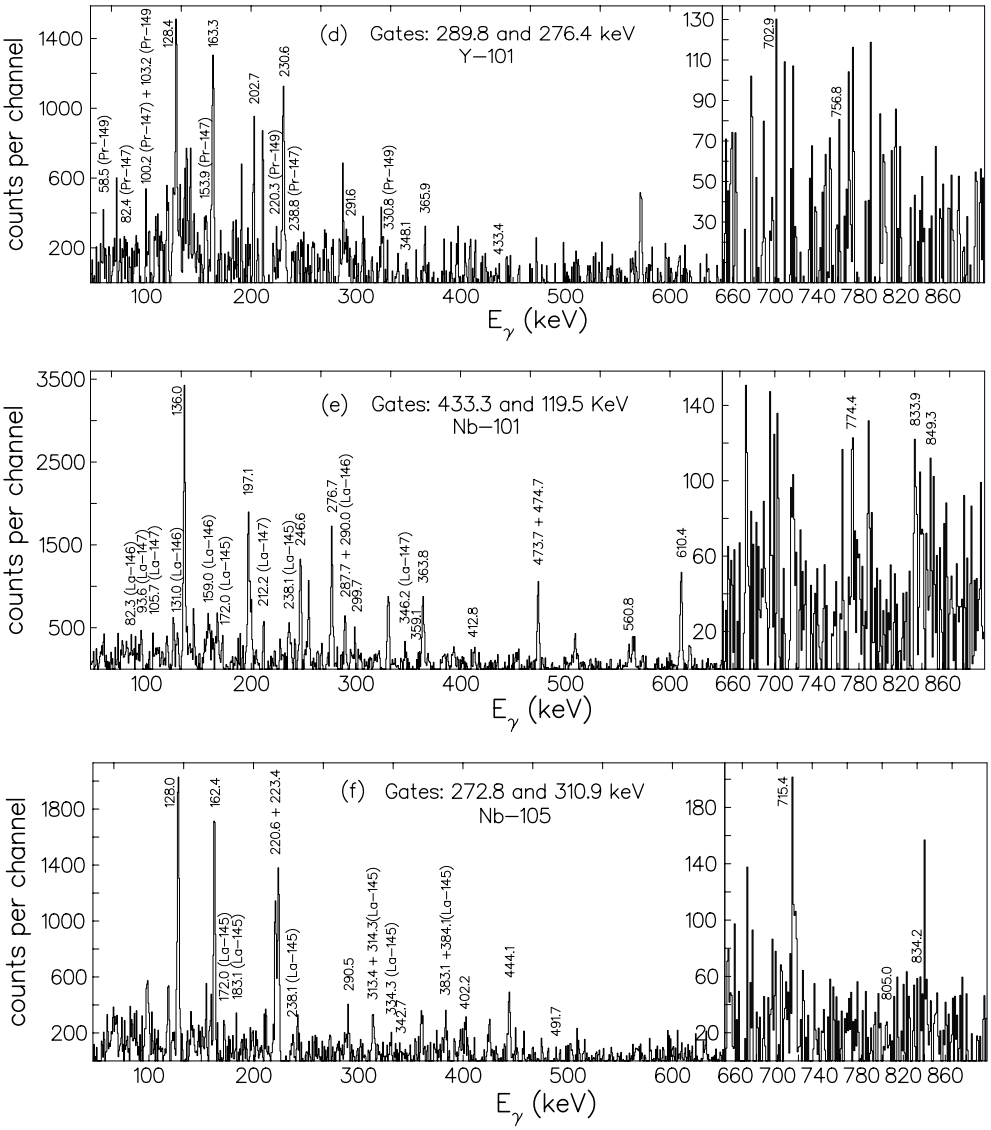

Figure 1. (Continued.)

are in all the double-gated spectra used for cross-checking the coincident relationship and for determinations of the transition energies and relative intensities. Figure 1(b) also shows the observations of the decay-out transitions, 1435.6 keV, 1166.1 keV, 882.8 keV and 546.1 keV of the 2142.1 keV $(17/2^+)$ isomer state in ^{99}Y. In figure 1(c) a gate was set on the 125.3 keV ground transition of ^{99}Y and the other on the strong 220.3 keV transition of its 4*n* fission partner ^{149}Pr, aiming to show the low-lying decay-out transitions of the band (4), the 1529.4 keV and 1370.9 keV transitions. Proper background-subtractions were always carefully made for every double-gated spectrum, which is of particular importance for fission data analysis. See the spectra and captions of figure 1 for more details.

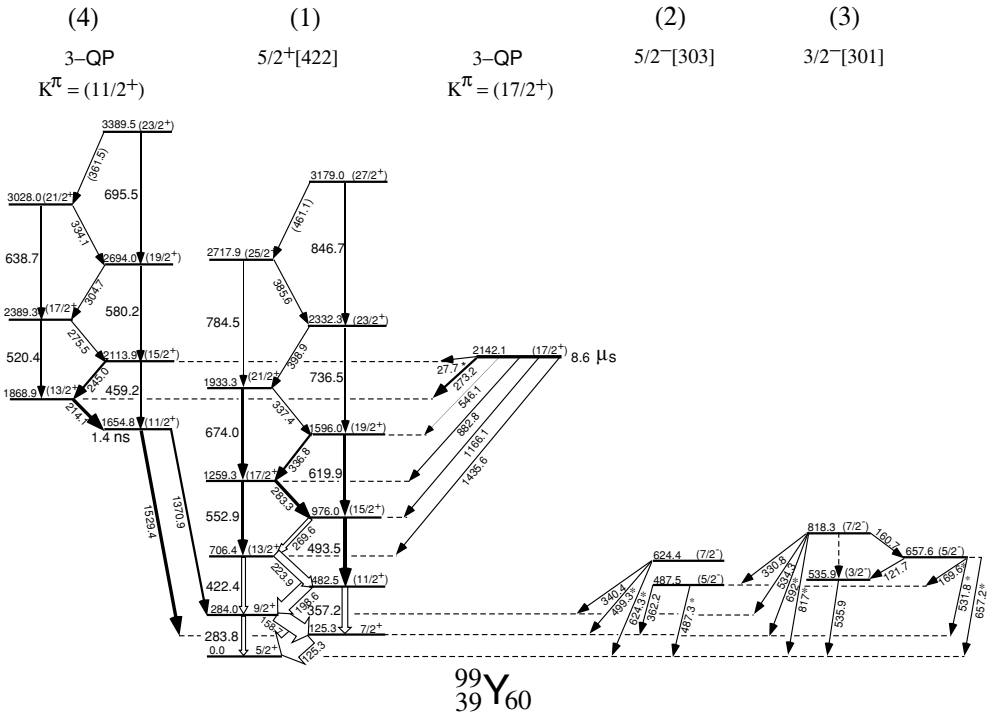

Figure 2. A new level scheme of ^{99}Y proposed in the present work. The transitions with asterisks in the level schemes indicate those reported by beta decay studies and related to the level or levels identified in the present fission work, but the transitions themselves not definitely identified in our experiment. The 27.7 keV transition decaying the 2142.1 keV $(17/2^+)$ isomer state reported in [21] is not observed in the present work due to the low-energy cut-off of the spectrometer.

3. Results and discussions

3.1. New level schemes, transition energies and relative intensities

Figures 2, 3, 4 and 5 show the new level schemes of ^{99}Y, ^{101}Y, ^{101}Nb and ^{105}Nb, respectively, proposed in the present work. The transitions with asterisks in the level schemes indicate those reported by beta decay studies and related to the level or levels identified in the present fission work, but the transitions themselves (with asterisk) not definitely identified in our experiment. The non-observations of the starred transitions are due to the fact that in the related triple-coincidence spectra at least one gate had to be set on the fission partner transitions, and the gamma peak under consideration in such gated spectra is not intense and/or not 'clean' enough to identify them, even though they were reported by β decay measurements to be more intense than those that are identified in the present work. The 27.7 keV decay-out transition of the 2142.1 keV $(17/2^+)$ isomer state in ^{99}Y is not observed in the present work because its transition energy is lower than the cut-off limit of the spectrometer.

It can be seen in figure 2 that band (1) of ^{99}Y previously reported in [8, 20, 21] is extended from $(19/2^+)$, 1596.0 keV up to $(27/2^+)$, 3179.0 keV. Band (4) is extended from $(15/2^+)$, 2113.9 keV up to $(23/2^+)$, 3389.5 keV. Bands (2) and (3) with 2–3 levels reported in [19] by means of decay study are observed by prompt gammas from fission for the first time in this work. The 8.6 μs isomer at 2142.1 keV reported in [21] is identified in the present work. The

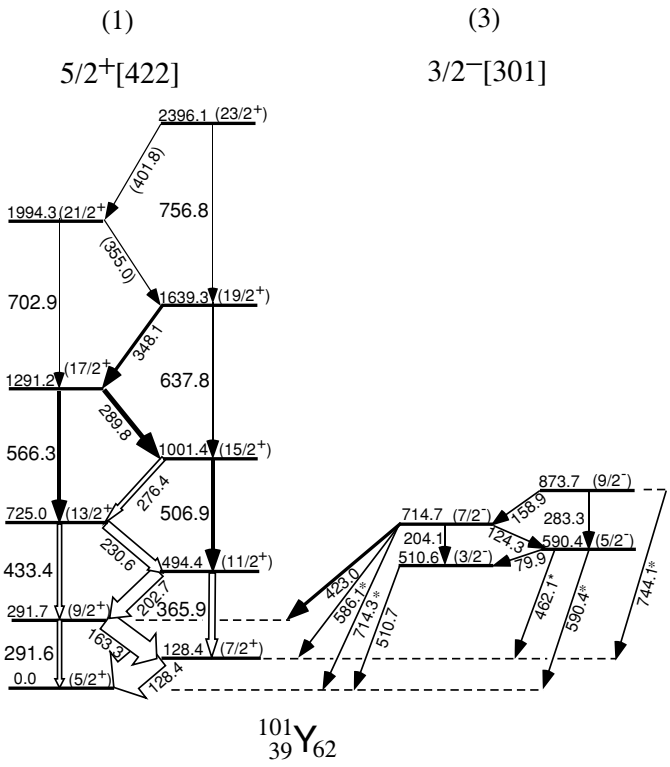

Figure 3. A new level scheme of ^{101}Y proposed in the present work. The transitions with asterisks in the level schemes indicate those reported by beta decay studies and related to the level or levels identified in the present fission work, but the transitions themselves not definitely identified in our experiment.

feedings from this isomer to the $13/2^+$, $15/2^+$, $17/2^+$ and $19/2^+$ levels of the ground-state band and to the $13/2^+$ level of band (4) are observed. It should be noted that this isomer state was certainly populated by fission; however, considering the lifetime of the isomer and the $\sim$1 μs coincidence resolving time, the observed cascades decaying out of the isomer state are not in prompt-coincidence with the corresponding fission partner transitions, and not with possible higher-lying transitions either. We tried to search the possible prompt structure built on the isomer but could not find any, which can be understood since the population of the isomer is found to be weak (see table 1 for relative intensities of the decay-out transitions of the isomer state determined in the present work).

In figure 3 band (1) of ^{101}Y previously reported in [8, 22, 23] is extended in this work from ($13/2^+$), 725.0 keV up to ($23/2^+$), 2396.1 keV. Band (3) with four levels observed in the decay work [19] is observed for the first time in fission in the present work.

The strongest population of three well-developed bands was seen in ^{101}Nb (see figure 4). Band (1) reported in [8, 19, 24] is extended in the present work from ($21/2^+$), 2072.7 keV up to ($27/2^+$), 3396.8 keV band (2) from ($21/2^-$), 2414.7 keV up to ($25/2^-$), 3206.8 keV and band (3) from ($11/2^-$), 1005.9 keV up to ($21/2^-$), 2624.2 keV.

For ^{105}Nb, the only reported band (1) is extended from ($15/2^+$), 1045.4 keV [8] up to ($25/2^+$), 2868.0 keV in the present work (see figure 5).

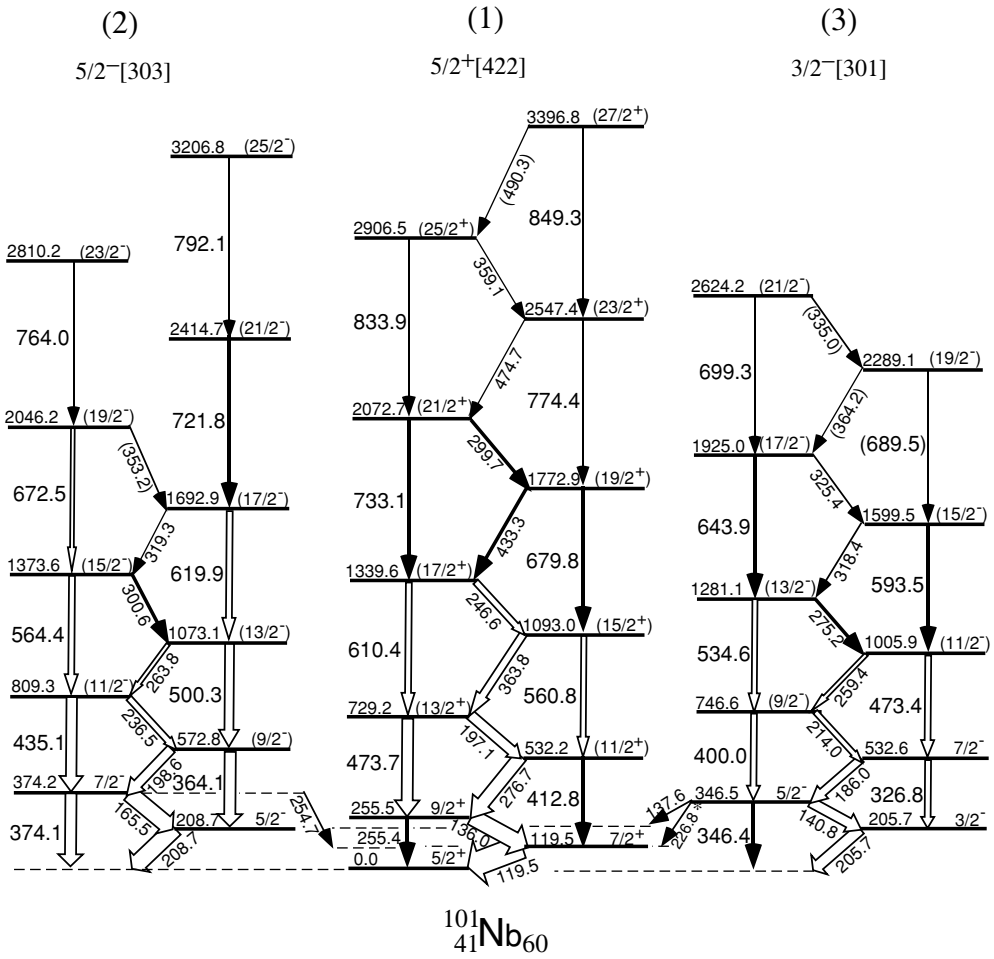

Figure 4. A new level scheme of ^{101}Nb proposed in the present work.

Tables 1, 2, 3 and 4 give the transition energies and relative intensities determined in ^{99,101}Y and ^{101,105}Nb, respectively. Also shown in the tables are those transitions obtained earlier by decay studies or by fission measurements reported by other authors [8, 19–24].

The systematic errors of the transition energy determinations are of the order of ±0.1 keV, and the systematic uncertainty of the relative photon intensities range from ∼3% for stronger peaks to ∼20% for weaker ones, and to even larger values for peak-overlapping cases. For some of the transitions, relative intensities are not given in the tables because reliable determinations of their relative transitions intensities could not be made due to serious peak-overlapping and/or their very small intensities.

3.2. Discussions and interpretations

3.2.1. ^{99,101}Y. Configurations are assigned to the extended bands in ^{99,101}Y following the results based on the particle-rotor model calculations for the low-spin part of ^{99,101}Y in [22, 23]

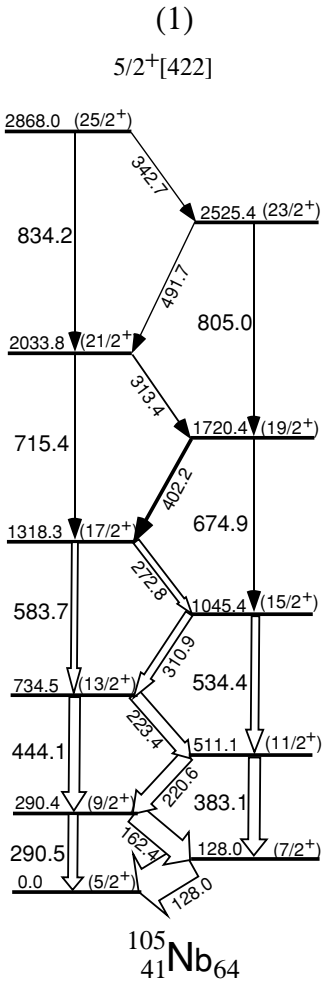

Figure 5. A new level scheme of ^{105}Nb proposed in the present work.

(see figures 2 and 3). An assignment of $\pi 5/2^+[422]\ \pi g_{9/2}$ to the ground-state band (1) in ^{99,101}Y, $\pi 5/2^-[303]$ and $\pi 3/2^-[301]\ \pi f_{5/2}$ to the two negative-parity side-bands, bands (2) and (3), identified in ^{99}Y, respectively, and the latter to the only side-band, band (3), observed in ^{101}Y. The ground-state bands of ^{99,101}Y, extended in the present work, are very similar to each other and exhibit properties of well-deformed prolate rotors. The characteristics of a well-deformed prolate rotor and the similarities of the ground-state band behaviour in the Y isotopes can be interpreted by the deformed shell gaps at $Z = 38$ and $N = 60$, 62. It is reasonable to consider ^{99,101}Y as a single quasi-proton coupled to the deformed cores ^{98}Sr and ^{100}Sr, respectively, where identical yrast bands are seen [4].

The identified 8.6 μs isomer at 2142.1 keV in ^{99}Y is found to be depopulated through transitions with similar intensities into the $13/2^+$, $15/2^+$, $17/2^+$ and $19/2^+$ (but not the $11/2^+$) levels of the ground-state band (see figure 2). Based on the above observations and the arguments of K-forbiddeness, the related formula $K^\pi = 17/2^+$ was proposed for this isomer

Table 1. Energies and relative intensities of the transitions observed in ^{99}Y.

E_γ (keV)	Relative intensities	E_γ (keV) [21]	E_γ^β (keV) [19]	Initial level (keV)	Half life (ns) [19]
		27.7		2142.1	8.6 μs
121.7			120.6	657.6	
125.3	100	125.1	125.1	125.3	0.047
158.7	54.2	158.7	158.6	284.0	
160.7			160.7	818.3	
			169.6	657.6	
198.6	35.6	198.5	198.5	482.5	
214.1	7.8	214.0		1868.9	
223.9	23.3	223.9		706.4	
245.0	3.6	245.2		2113.9	
269.6	10.7	269.6		976.0	
273.2	2.4	272.9		2142.1	8.6 μs
275.5	1.8			2389.3	
283.3	7.6	283.5		1259.3	
283.8	9.6	283.8	283.7	284.0	
304.7	1.1			2694.0	
330.8			330.3	818.3	
334.1	0.6			3028.0	
336.8	4.2	336.3		1596.0	
337.4	2.2			1933.3	
340.4			340.8	624.4	
357.2	12.5	357.2	357.2	482.5	
(361.5)				3389.5	
362.2			362.1	487.5	
385.6				2717.9	
398.9	1.6			2332.3	
422.4	10.6	422.3		706.4	
459.2	2	459.2		2113.9	
(461.1)				3179.0	
			487.3	487.5	
493.5	6.8	493.5		976.0	
			499.3	624.4	
520.4	1.8			2389.3	
			531.8	657.6	
534.3			533.9	818.3	
535.9			536.1	535.9	
546.1	0.3	546.2		2142.1	8.6 μs
552.9	4.4	553.2		1259.3	
580.2	1.2			2694.0	
619.9	2.6	619.7		1596.0	
			624.3	624.4	
638.7	1.1			3028.0	
674.0	2.8			1933.3	
			692.0	818.3	
695.5	0.9			3389.5	
736.5	1.2			2332.3	
784.5	1.1			2717.9	
			817.0	818.3	
846.7	0.9			3179.0	
882.8	1.8	882.5		2142.1	8.6 μs
1166.1	0.9	1166.0		2142.1	8.6 μs
1370.9	2.8	1371.0		1654.8	
1435.6	1.4	1435.5		2142.1	8.6 μs
1529.4	6.2	1529.5		1654.8	

Table 2. Energies and relative intensities of the transitions observed in ^{101}Y.

E_γ (keV)	Relative intensities	E_γ (keV) [8]	E_γ^β (keV) [19]	Initial level (keV)
79.9			79.7	590.4
124.3			124.0	714.7
128.4	100	128.2	128.3	128.4
158.9			158.4	873.7
163.3	48.8	163.4	163.4	291.7
202.7	30.2	202.6	202.6	494.4
204.1			203.9	714.7
230.6	21.3	230.7	230.7	725.0
276.4	10.4			1001.4
283.3			282.7	873.7
289.8	6.4			1291.2
291.6	10.8	291.6	291.7	291.7
348.1	2.4			1639.3
(355.0)				1994.3
365.9	11.6	366.0	366.0	494.4
(401.8)				2396.1
423.0	2.8		422.8	714.7
433.4	9.9	433.3		725.0
			462.1	590.4
506.9	4.9			1001.4
510.7			510.7	510.6
566.3	4.2			1291.2
			586.1	714.7
			590.4	590.4
637.8	1.8			1639.3
702.9	1.2			1994.3
			714.3	714.7
			744.1	873.7
756.8				2396.1

state. A three-qp configuration $\pi 5/2[422]\upsilon 3/2[411]\upsilon 9/2[404]$ was assigned to this level (see [21]).

It is worthwhile noting the band (band (4)) built at the excited $11/2^+$ state with excitation energy as high as 1654.8 keV in ^{99}Y which is well developed in the present work (see figure 2). This band de-excites via a 1529.4 keV transition to the $7/2^+$ state, and a weaker 1370.9 keV transition to the $9/2^+$ state of the ground-state band, just opposite to what was observed in the side-bands in the Tc and Rh isotopes (see [17, 18]), where the side-band built on an excited $11/2^+$ level with low excitation energy (∼570–770 keV) predominantly feeds the $9/2^+$ state and very weakly the $7/2^+$ state of the yrast bands in Tc and Rh isotopes, providing strong evidences of triaxiality in the nuclei [17, 18]. However, this band (4) is not an analogous collective side-band to the ground band as in Rh nuclei, because its half life of 1 ns for the $11/2$ bandhead represents a retardation of three orders of magnitude if M1 or two orders of magnitude if E2. As can be seen in figure 2, the 8.6 μs isomer state also feeds, via 27.7 keV and 273.2 keV transitions, respectively, the 2113.9 keV level and the 1868.9 keV level of band (4). Based on the measurements of total internal conversion coefficients of this 27.7 keV low-energy transition, on the 1.4 ns lifetime determined for the 1654.8 keV level, and the high-energy decay-out transitions of 1529.4 keV and 1370.9 keV feeding the $7/2^+$ and $9/2^+$

Table 3. Energies and relative intensities of the transitions observed in ^{101}Nb.

E_γ (keV)	Relative intensities	E_γ (keV) [24]	E_γ^β (keV) [19]	Initial level (keV)	Half life (ns) [19]
119.5	100	119.3	119.3	119.5	0.084
136.0	64	135.9	135.9	255.5	0.035
140.8	14.1	141.5	140.6	346.5	0.024
165.5	29.2	165.7	165.8	374.2	0.019
186.0	9.5	186.2	186.0	532.6	0.013
197.1	20.7	197.0	197.7	729.2	
198.6	17.6	198.6		572.8	
205.7	21.3	205.6	205.6	205.7	
208.7	36.4	208.5	208.5	208.7	
214.0	5.9	214.1		746.6	
			226.8	346.5	
236.5	7.2	236.5		809.3	
246.6	7.2	246.6		1339.6	
255.4	6.8	255.2	255.2	255.5	
259.4	5.3	259.4		1005.9	
263.8	4.5	263.9		1073.1	
275.2	3.3			1281.1	
276.7	30.3	276.8		532.2	
299.7	2.4			2072.7	
300.6	3.6			1373.6	
318.4	1.9			1599.5	
319.3	1.1			1692.9	
325.4	1.6			1925.0	
326.8	2.9	327.7	327.1	532.6	
(335.0)				2624.2	
346.4	3.4			346.5	
(353.2)				2046.2	
359.1				2906.5	
363.8	12.8	364.1		1093.0	
364.1	20.8	364.4		572.8	
(364.2)				2289.1	
374.1	19.5			374.2	
400.0	7.6	400.3		746.6	
412.8	5.8	412.7		532.2	
433.3	3.7	433.0		1772.9	
435.1	18.8	435.1		809.3	
473.4	7.1	473.5		1005.9	
473.7	19	474.1		729.2	
474.7	1.1			2547.4	
(490.3)				3396.8	
500.3	17.2	500.4		1073.1	
534.6	5.3			1281.1	
560.8	4.4	561.4		1093.0	
564.4	10.9	564.4		1373.6	
593.5	3.6			1599.5	
610.4	9.4	610.7		1339.6	
619.9	9.6	620.1		1692.9	
643.9	3.1			1925.0	
672.5	4.5			2046.2	
679.8	2.4	679.6		1772.9	
689.5	0.9			2289.1	

Table 3. (Continued).

E_γ (keV)	Relative intensities	E_γ (keV) [24]	E_γ^β (keV) [19]	Initial level (keV)	Half life (ns) [19]
699.3	1.4			2624.2	
721.8	3.4	722.0		2414.7	
733.1	3.2	733.0		2072.7	
764.0	1.1			2810.2	
774.4	1.1			2547.4	
792.1	0.9			3206.8	
833.9	1.8			2906.5	
849.3	0.6			3396.8	

Table 4. Energies and relative intensities of the transitions observed in ^{105}Nb.

E_γ (keV)	Relative intensities	E_γ (keV) [8]	E_γ^β (keV) [19]	Initial level (keV)
128.0	100	127.9		128.0
162.4	66.3	162.3		290.4
220.6	36.4	220.8		511.1
223.4	17.9	223.6		734.5
272.8	5.5			1318.3
290.5	11.4	290.2		290.4
310.9	11.7	311.0		1045.4
313.4	1.1			2033.8
342.7				2868.0
383.1	13.8	383.1		511.1
402.2	3.1			1720.4
444.1	14.1	444.4		734.5
491.7				2525.4
534.4	8.5	534.6		1045.4
583.7	6.4			1318.3
674.9	2.2			1720.4
715.4	1.5			2033.8
805.0	0.9			2525.4
834.2	1			2868.0

level of the ground-state band, respectively, $K^\pi = 11/2^+\{\pi 5/2[422]\upsilon 3/2[411]\upsilon 9/2[404]\}$ was assigned to the 1654.8 keV level [21]. In the present work the non-observation of the 1654.8 keV transition between the 1654.8 keV level and the ground state ($5/2^+$) supports this assignment. The positive-parity rotational band, band (4), built on this 1654.8 keV, ($11/2^+$) level reaching 3389.5 keV, ($23/2^+$) identified in the present work is thus a three-qp band.

3.2.2. ^{101,105}Nb. The ground-state band (1) and the two side-bands of ^{101}Nb, bands (2) and (3), are extended up to higher excitations in the present work (see figure 4), with the two side-bands reaching much higher excitations and spins than those in the Y isotopes. However, the population of ^{105}Nb is much weaker, with only one band, band (4), observed (see figure 5). Following the assignments for Y isotopes, the ground-state bands in ^{101,105}Nb were assigned the $\pi 5/2^+[422]$ configuration, while $\pi 5/2^-[303]$ and $\pi 3/2^-[301]$ were assigned to the two side-bands in ^{101}Nb, respectively.

The interpretation of the ground-state bands in Nb isotopes as having the same configurations as those of ^{99,101}Y can be justified as follows: the quadrupole deformation

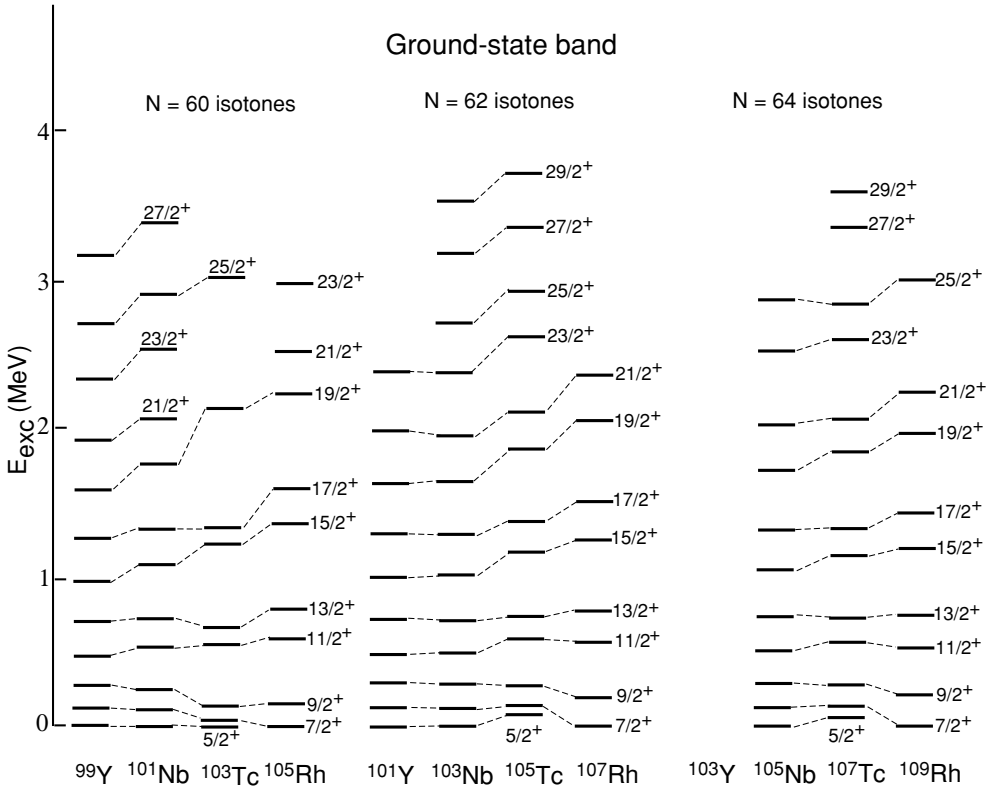

Figure 6. Level systematics of ground-state bands of $N = 60$, 62 and 64 isotones with odd-Z ranging from 39 to 45. The data of ^{103}Nb are taken from [25], ^{103}Tc from [13], ^{105,107}Tc from [18], ^{105}Rh from [14] and ^{107,109}Rh from [16].

in the region of $Z = 39$–45 is found to decrease with increasing Z (see section 4), following the same trend observed in even-Z nuclei in the region of $Z = 38$–42 (see e.g. [8]). In the Nilsson diagram for the $Z \sim 40$ region, one can see a crossing between the upsloping $3/2^-[301]$ and downsloping $5/2^+[422]$ orbital above the $Z = 38$ deformed shell gap. So for $Z = 41$ (Nb) with lower deformation than $Z = 39$ (Y) the odd proton can occupy the $5/2^+[422]$ orbital with the $3/2^-[301]$ lying below the Fermi level; and for $Z = 39$ (Y) with larger deformation the odd proton can also occupy the $5/2^+[422]$ orbital, while the $3/2^-[301]$ lies above the Fermi level.

3.3. Triaxiality trends in the odd-A isotopes of Y(39)–Nb(41)–Tc(43)

Since a transition from the axially symmetric shape in Zr ($Z = 40$) to triaxiality in Mo ($Z = 42$) isotopes was identified [10] in the even-Z nuclei and triaxial deformations were observed in the heavier odd-Z nuclei with $Z = 43$ (Tc) and $Z = 45$ (Rh) [13–17], the present spectroscopic information of the Y ($Z = 39$) and Nb ($Z = 41$) isotopes may allow searches for the expected triaxiality shape transition in the $Z = 39$ (Y)–41 (Nb)–43 (Tc) nuclei in this important region.

Figure 6 shows the level systematics of the positive-parity ground-state bands in $N = 60$, 62 and 64 isotonic chains with odd-Z ranging from 39 to 45. In this figure a distinct difference in level pattern can be seen between the Y and the Tc and Rh isotones. An almost equally

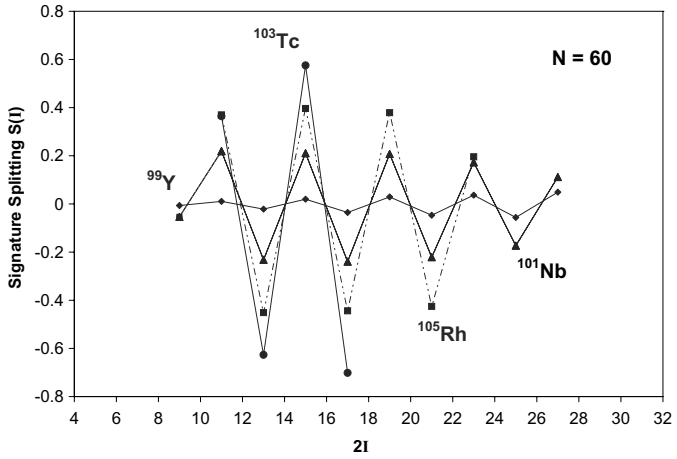

Figure 7. Variations of signature splitting $S(I)$ with spins of the ground-state bands in $N = 60$ isotones with odd-$Z = 39$–45. The data of ^{103}Tc and ^{105}Rh are taken from [13] and [14], respectively. ♦ ^{99}Y, ▲ ^{101}Nb, ● ^{103}Tc, ■ ^{105}Rh.

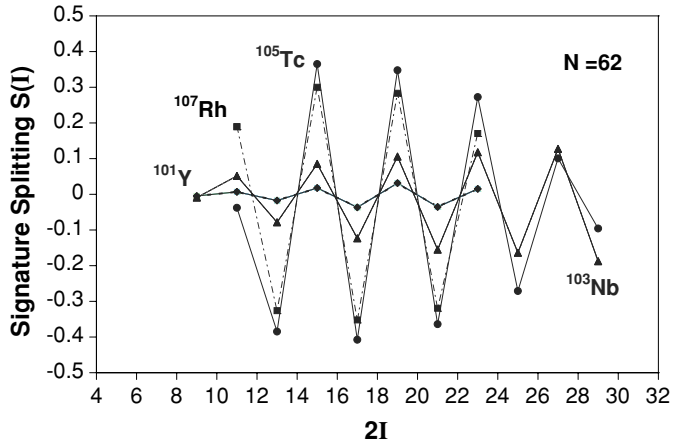

Figure 8. Variations of signature splitting $S(I)$ with spins of the ground-state bands in $N = 62$ isotones with odd-$Z = 39$–45. The data of ^{103}Nb, ^{105}Tc and ^{107}Rh are taken from [25], [18] and [16], respectively. ♦ ^{101}Y, ▲ ^{103}Nb, ● ^{105}Tc, ■ ^{107}Rh.

spaced level pattern is seen in Y, while level bunching in Tc and Rh isotones is observed. The difference can be more clearly seen in figures 7 and 8, which show signature-splitting functions $S(I)$ of the positive-parity ground-state bands of $N = 60$ and $N = 62$ isotones, respectively, in this odd-Z range of $Z = 39$–45. Here we use the signature-splitting function $S(I)$ used in [17, 18] given by Gelberg *et al*. The signature splitting $S(I)$ is defined as

$$S(I) = \frac{E(I) - E(I-1)}{E(I) - E(I-2)} \frac{I(I+1) - (I-2)(I-1)}{I(I+1) - (I-1)I} - 1. \tag{1}$$

For both the $N = 60$ and $N = 62$ isotonic chains the pronounced difference in $S(I)$ between the Y and the Tc and Rh isotones is clearly seen. Very small signature splitting is observed

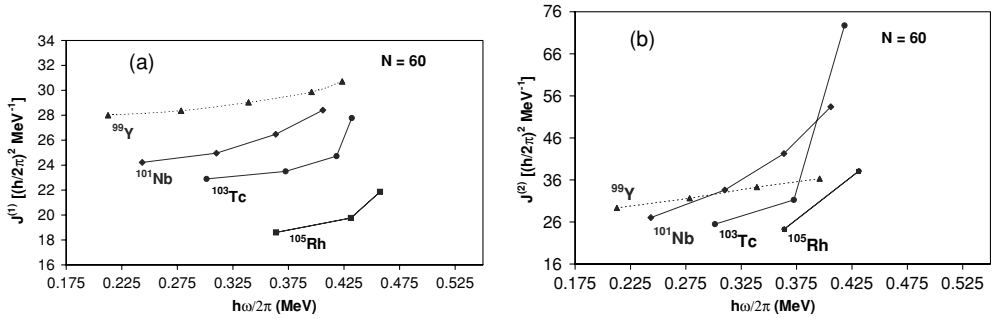

Figure 9. Kinematic (a) and dynamic (b) moments of inertia of the ground-state bands of $N = 60$ isotones with odd-$Z = 39$–45. The data of ^{103}Tc are taken from [13] and ^{105}Rh from [14].

in Y, in pronounced contrast to the quite large splittings in the Tc and Rh isotones. In fact $S(I)$ increases significantly from $\sim \pm(0.02$–$0.04)$ in ^{99,101}Y to $\sim \pm(0.40$–$0.60)$ in ^{103,105,107,109}Tc and $\sim \pm(0.20$–$0.40)$ in ^{105,107,109,111,113}Rh. Since large triaxial deformation has been reported in the Tc and Rh isotopes and the signature-splitting function $S(I)$ is very sensitive to triaxiality, the above observations indicate that, while triaxial deformation plays a significant role in the Tc and Rh isotopes [17, 18], mainly axially symmetric deformed shapes remain in ^{99}Y, implying a shape transition from the axially symmetric deformed shape in $Z = 39$ isotopes to triaxial deformations in $Z = 43$, 45 isotopes (see the following section for detailed discussions based on model calculations). It should be noted that the difference in the signature splitting between Y ($Z = 39$) and Tc ($Z = 43$), Rh ($Z = 45$) discussed above is in fact even more pronounced than that reported for the $\upsilon h_{11/2}$ band of the even–odd neighbours ^{101}Zr and ^{103}Mo [10], which was attributed to a triaxial degree of freedom in ^{103}Mo and the axially symmetric shape in ^{101}Zr by performing particle-rotor model calculations [10]. It can also be seen from figures 7 and 8 that the Nb isotones have intermediate values of signature-splitting functions $S(I) \sim \pm(0.10$–$0.20)$ between those of Y and Tc, Rh isotones, which may imply a transitional character for the Nb isotones with regard to triaxial deformation. This deduction is also supported by the model calculations in the following section.

The fission of ^{252}Cf does not populate sufficiently high excitations and spin states to allow observations of the complete band crossings in these Y and Nb isotopes. However, the variations of the kinematic and dynamic moments of inertia versus rotational frequencies for ground-state bands of the $N = 60$ isotones with odd-Z shown in figures 9(a) and (b), respectively, and those of $N = 62$ isotones in figures 10(a) and (b) indicate a clear tendency for the crossing frequencies of Rh ($Z = 45$) and Tc ($Z = 43$) to be lower than that of Y ($Z = 39$) isotones. This behaviour is similar to the case of the $\upsilon h_{11/2}$ band in the neighbouring even–even Zr and Mo isotopes ($N = 60$, 62), where a shift of band crossing to lower rotational frequency observed in the $\upsilon h_{11/2}$ bands of Mo compared to Zr isotopes was accounted for by triaxiality in Mo and the axially symmetric shape in Zr isotopes in CSM calculations [10]. Despite the fact that the bands of Y isotopes do not extend to high enough spins to allow a similar CSM calculation to address the difference in the band crossing in terms of triaxiality, the similar shift of band crossing observed in Y compared to Tc and Rh isotopes supports the interpretation of the axially symmetric shape in Y isotopes. It can also be seen in figures 9 and 10 that the crossing frequencies of Nb isotones is likely between the values of Y and Tc, Rh isotones, which may also suggest a transitional character for Nb isotones with regard to triaxial deformation.

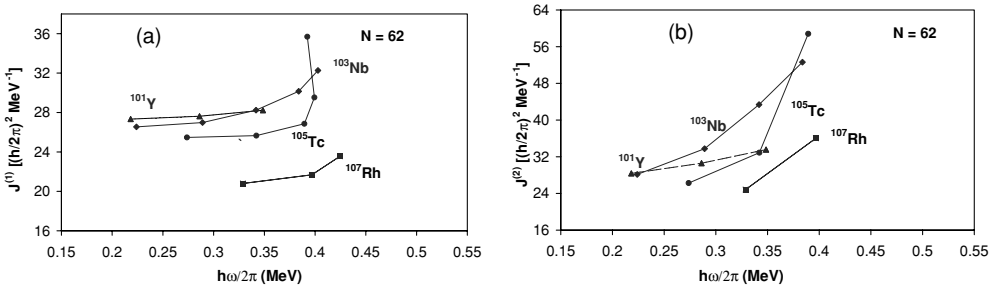

Figure 10. Kinematic (a) and dynamic (b) moments of inertia of the ground-state bands of $N = 62$ isotones with odd-$Z = 39$–45. The data of ^{103}Nb are taken from [25], ^{105}Tc from [18] and ^{107}Rh from [16]. ▲ ^{101}Y, ♦ ^{103}Nb, ● ^{105}Tc, ■ ^{107}Tc.

4. Rigid triaxial-rotor-plus-quasiparticle model calculations

In previous publications [17, 18] we have described the rigid triaxial-rotor-plus-quasiparticle model. Therefore, in the present paper we will mention only a few basic features of this model. A more detailed description can be found in the seminal paper by Larsson *et al* [29]. By 'rigid' we mean that the shape, which is defined by the deformation parameters of the core [30], is the same for all states. The deformation parameters are fixed, and this model does not contain either β or γ vibrations.

The single-particle Hamiltonian contains an anisotropic oscillator potential, which depends on the deformation parameters ε_2 and γ. We use the Lund convention for γ, which is confined to the 0 to -60° interval. The program uses the so-called standard Nilsson parameters [30]. The Hamiltonian also includes a pairing interaction. As input, only pairing strengths are given. Quasiparticle energies, the pairing gap and the Fermi energy are calculated by the code, as explained in [29]. The basis on which the total Hamiltonian is diagonalized contains up to 15 Nilsson orbitals. The deformation induces a mixing of the spherical single-particle configurations. If the nucleus is not axially symmetric, the mixing of orbitals with different values of Ω can be quite strong. There is practically no free parameter in the quasiparticle Hamiltonian.

We used the hydrodynamical irrotational flow formula for the ratios of the three moments of inertia [17, 31]. The moments of inertia were normalized by using an effective $E(2^+)$ core energy, which is not directly related to the actual energy of the core 2^+ state. It is, in fact, only a scaling factor, which has been fitted to the excitation energies of the odd nucleus.

Since $E(2^+)$ is only a scaling factor, its variation alone cannot achieve a good energy fit. The next step in the energy fit is the variation of ε_2. The final step is the fit of the signature splitting, which depends mainly on γ. After repeating this procedure several times, a satisfactory fit of excitation energies can be obtained. The branching ratios represented a further possibility of improving the overall fit or, at least, a consistency check.

A Coriolis attenuation factor of 0.8 to 1.0 has been used for 'fine tuning'. Its effect on the observables is rather weak.

The fitted parameters are summarized in table 5, and figure 11 indicates the spherical single-particle levels used in the calculations.

Before proceeding further, we must make a remark on the validity of the model at relatively high spins. In our previous studies, especially in those of ^{111,113}Rh, a band crossing was clearly visible at spins around 23/2. This was interpreted as the crossing of the one-quasiparticle ground band with a three-quasiparticle band based on a $\pi\, g_{9/2}\, \upsilon h_{11/2}{}^2$ configuration. In contrast,

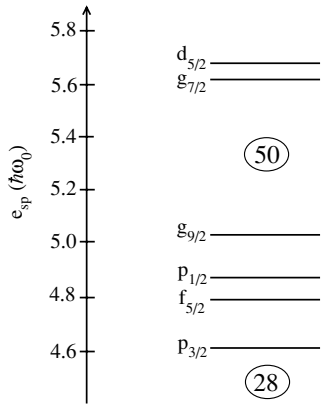

Figure 11. Spherical single-particle levels used in the triaxial-rotor-plus-particle model calculations in the present work.

Table 5. Model calculation parameters for Y and Nb isotopes.

Nucleus and band	Quadrupole deformation ε_2	Triaxiality γ (°)	Coriolis attenuation factor ξ	Inertial parameter $E(2^+)$ (MeV)
^{99}Y $5/2^+[422]$ band	0.41	0	1.0	0.14
^{101}Y $5/2^+[422]$ band	0.39	0	0.95	0.16
^{101}Nb $5/2^+[422]$ band	0.35	−19	0.83	0.2
$5/2^+[422]$ band	0.36	−14	0.8	0.16
$3/2^-[301]$ band	0.25	−5	1.0	0.13
$5/2^-[303]$ band	0.25	−5	1.0	0.13
^{103}Nb $5/2^+[422]$ band	0.37	−15	0.8	0.155
^{105}Nb $5/2^+[422]$ band	0.36	−13	0.8	0.16

we do not see any clear indication of backbending in the Y and Nb nuclei as mentioned above. Therefore, one is tempted to consider the observed cascades, with spins up to $I = 27/2$, as one-quasiparticle rotational bands. It is more plausible to assume that also in this case we deal with band mixing. The mixing matrix elements are probably stronger than in the Rh nuclei studied in [17], so that the mixing is distributed over several states. This may be the reason for seeing only a smooth transition. In practical terms, this means that the calculated wavefunctions and excitation energies can be taken at a face value only below $I = 23/2$.

We will first consider the lowest-Z nucleus here, ^{99}Y ($Z = 39$). Figure 12 shows a comparison of the calculated signature splitting with the experiment for the ground-state band of ^{99}Y. The calculations were performed for axial symmetry ($\gamma = 0°$) and for small triaxiality ($\gamma = -12.5°$). The axially symmetric calculation is obviously satisfactory for low spins up to $I = 19/2$. At higher spin, the experimental signature-splitting function $S(I)$ (expressed in equation (1)) is of the same sign, but significantly smaller than in the calculation for axial symmetry. Similar deviations of experiment from the theory at higher spins were also noticed in our previous papers on Rh and Tc [17, 18]. In the latter cases, the deviation was associated with the sharp backbending and attributed to the alignment of a pair of $h_{11/2}$ neutrons. As noticed above, in this case the $h_{11/2}$ neutrons are also expected to be major participants in carrying angular momentum along the rotation axis. Since signature splitting in an axially symmetric nucleus can be considered as a consequence of Coriolis coupling, the lowered value of $S(I)$ at the higher spins could also be attributed to a decrease of the summed Coriolis matrix

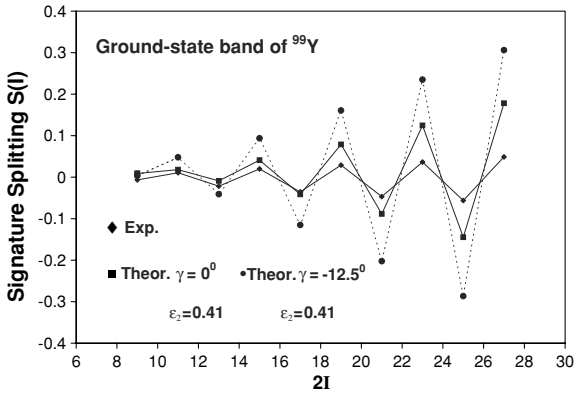

Figure 12. Triaxial-rotor-plus-particle model calculations for the signature splitting of the ground-state band of ^{99}Y. The calculations are performed with $\varepsilon_2 = 0.41$, $\gamma = 0^\circ$, $\xi = 1.0$, $E(2^+) = 0.14$ MeV (■) and $\varepsilon_2 = 0.41$, $\gamma = -12.5^\circ$, $\xi = 1.0$, $E(2^+) = 0.15$ MeV (●), respectively. Experimental values are indicated by ♦.

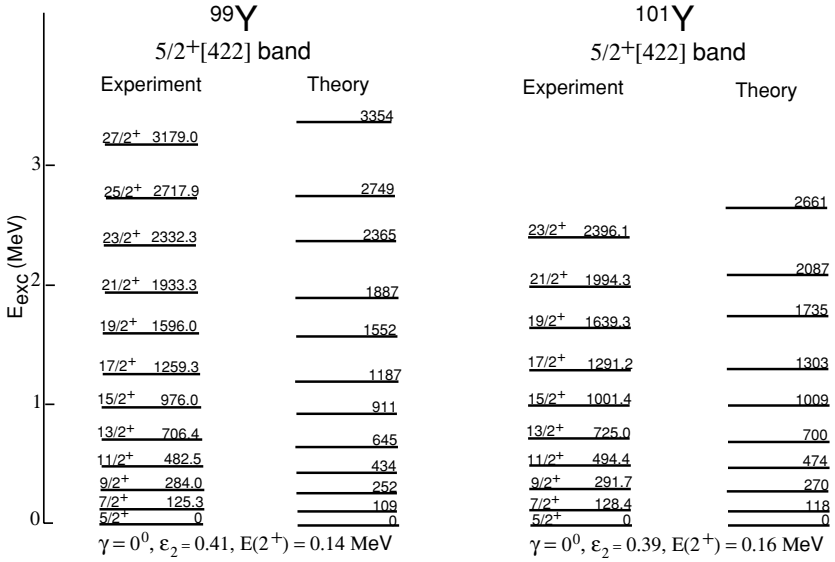

Figure 13. The comparison of experiment and theory for excitation energies of the ground-state bands in ^{99}Y and ^{101}Y. As in figure 12 the model calculations assume axial symmetry but are made with the same code and shell-model parameters as the triaxial rotor calculations.

elements as spin increases. Another characteristic is the quite small value of $S(I)$, which already points at axial symmetry.

The theoretical excitation energies in ^{99}Y and ^{101}Y are compared with the experiment in figure 13. We consider the fit at lower spins satisfactory. The calculation assumes a constant moment of inertia, so that this overall fit does not reproduce the experimental increase of the moment of inertia at higher spin.

In table 5, we fitted a quadrupole deformation $\varepsilon_2 = 0.41$ for the ground-state band of ^{99}Y, which roughly corresponds to $\beta_2 = 0.456$. If we look at the deformation parameters of

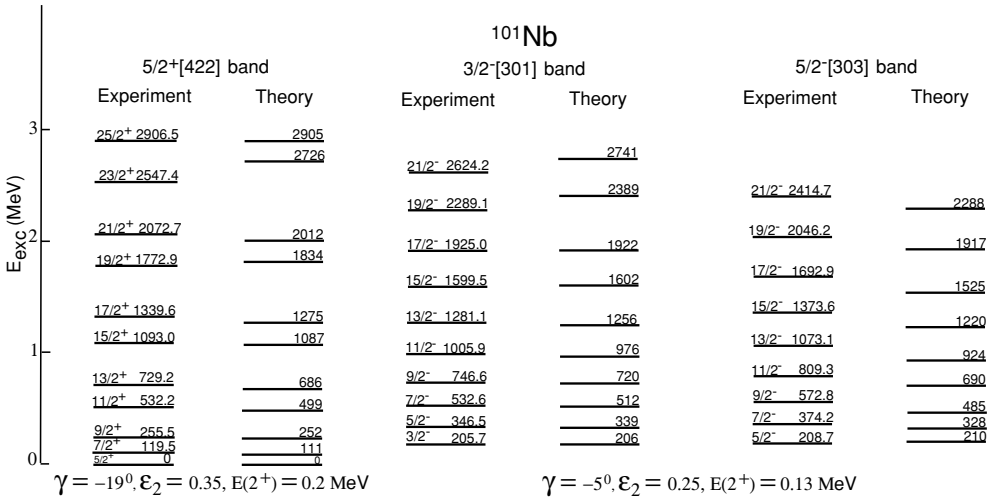

Figure 14. Experimental and theoretical energy comparisons for three bands in ^{101}Nb, namely, positive-parity ground $5/2^+[422]$ band and negative-parity excited $3/2^-[301]$ and $5/2^-[303]$ bands. The model calculations use a triaxiality γ parameter of -19° for the $5/2^+$ ground band and γ parameters of -5° for the negative-parity bands.

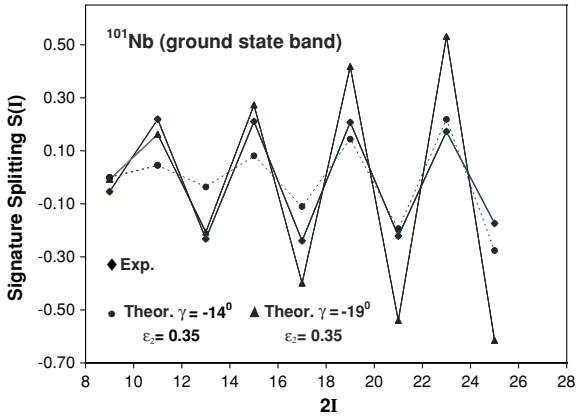

Figure 15. The signature-splitting plot for the ^{101}Nb $5/2^+$ ground-state band. The fit for $\gamma = -19^\circ$ is judged better than that for -14° at low spins and vice versa for the higher spins. See discussion in text.

the neighbouring even–even nuclei, we find $\beta_2 = 0.408(6)$ and $\beta_2 = 0.423$ for ^{98}Sr and ^{100}Sr, respectively [32]. This means that the fitted value of β_2 is plausible. ^{101}Y has been fitted with similar parameters and a similar result is obtained (see table 5 and figure 13).

Let us now examine the $Z = 41$ Nb nuclei. Here we have treated bands of both parities. Figure 14 gives an overview of the comparisons with experiment for excitations of the three bands in ^{101}Nb. In order to describe correctly the excitations and signature splitting (see below) in ^{101}Nb, we had to use a triaxiality parameter $\gamma = -19^\circ$ for the $5/2^+$ positive-parity band, and $\gamma = -5^\circ$ for the two negative-parity bands.

The signature splitting at low spins of the ground-state band in ^{101}Nb is quite reasonably reproduced with $\gamma = -19^\circ$ (see figure 15), but at high spins the theoretical values are again

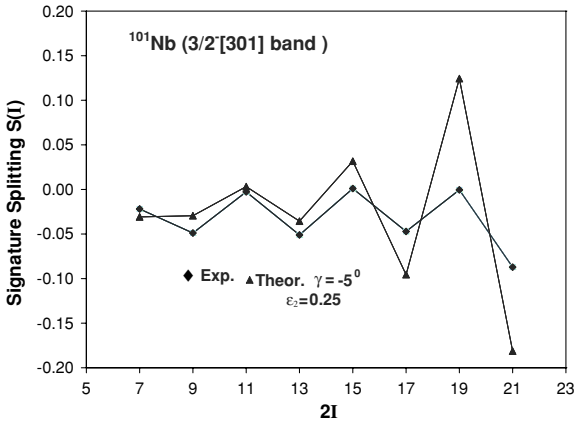

Figure 16. The signature-splitting plot for the ^{101}Nb $3/2^-[301]$ band with the best theoretical fit at lower spins coming at γ of -5°.

Table 6. Experimental and theoretical branching ratios for positive-parity bands in ^{99}Y and ^{101}Nb.

	^{99}Y		^{101}Nb	
Intensity ratio	Experiment	Theory	Experiment	Theory
$I(9/2 \to 5/2)/I(9/2 \to 7/2)$	0.18	0.23	0.11	0.25
$I(11/2 \to 7/2)/I(11/2 \to 9/2)$	0.35	0.56	0.19	0.63
$I(13/2 \to 9/2)/I(13/2 \to 11/2)$	0.46	1.07	0.92	1.75
$I(15/2 \to 11/2)/I(15/2 \to 13/2)$	0.64	1.61	0.34	1.53

too high. For the negative-parity bands we fitted $\gamma = -5^\circ$. As shown in figure 16, the experimental signature splitting for the negative-parity band based on $3/2^-[301]$ is quite small and well reproduced with $\gamma = -5^\circ$. The previously mentioned overestimation can be noticed again at higher spins. The generally small signature splitting in the negative-parity bands is understood in terms of the availability of comparable coupling to the $K = 1/2$ bands in the near-lying orbitals with the j values of $1/2$, $3/2$ and $5/2$. The admixture to $j = 3/2$ will give a signature-splitting contribution of opposite sign to the other two orbitals. We would, of course, not claim a rigid shape with $\gamma = -5^\circ$, but the model calculations may simulate other degrees of freedom, e.g. γ vibrations around a prolate, axially symmetric minimum.

In order to fit the ground-state band excitation energies in ^{103}Nb and ^{105}Nb, we took $\gamma = -15^\circ$ and $\gamma = -13^\circ$, respectively (see figure 17). The corresponding signature splittings can be seen in figures 18 and 19. In contrast to the negative-parity bands in ^{101}Nb, we can consider the positive-parity bands in ^{101}Nb, ^{103}Nb and ^{105}Nb as really displaying triaxial deformation.

The comparison between theoretical and experimental branching ratios shows a rather poor agreement, although the general trends are reproduced. As an example, we show several branching ratios in ^{99}Y and ^{101}Nb in table 6.

It is interesting to examine the systematics of the ε_2 and γ deformation parameters for the neutron-rich nuclei of $Z = 39$ to $Z = 45$ shown in figure 20. We can see that when going from $Z = 39$ to $Z = 45$, with neutron numbers roughly between 60 and 70, the ε_2 deformation parameter decreases from values slightly above 0.40 to 0.27. This trend can be understood, at least at a qualitative level. Due to the large value of N, the 'quasimagic' $Z = 40$ does not

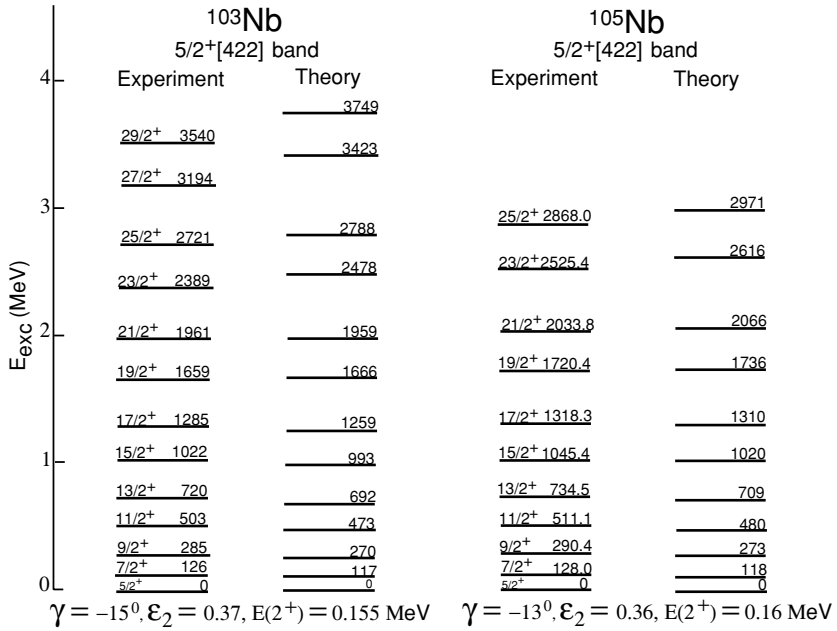

Figure 17. Ground-state band energy comparisons between experiment and theory for ^{103,105}Nb. The data of ^{103}Nb are taken from [25].

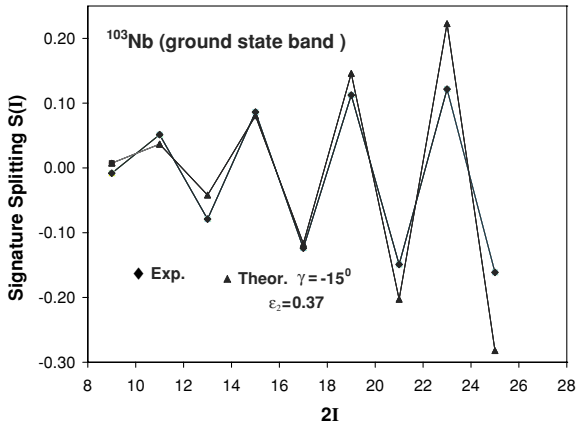

Figure 18. Signature-splitting comparison plots for the ^{103}Nb ground-state band. The data of ^{103}Nb are taken from [25]. Theoretical calculations used $\varepsilon_2 = 0.37$ and $\gamma = -15^\circ$. The fit is unusually good over the full range of spins, although theory overestimates splitting somewhat at higher spins.

manifest itself. Therefore, when Z decreases from 45 to 39, the proton number reaches the middle of the $Z = 28$–50 shell, the deformed shell gap at $Z = 38$, and this causes an increase in deformation. This increase in collectivity can be related to the increase of $N(\pi)N(\upsilon)$, i.e. of the product of the valence proton and neutron numbers (particles or holes) [33]. In the present case, this product obviously increases when we go from Rh to Y.

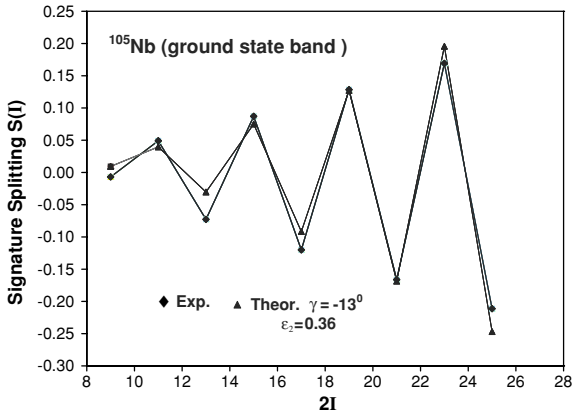

Figure 19. Same as figure 18 except for ^{105}Nb and $\gamma = -13^{\circ}$, $\varepsilon_2 = 0.36$.

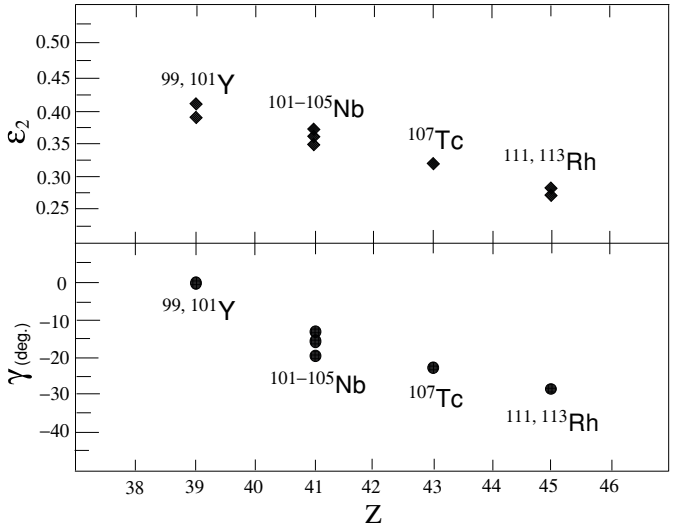

Figure 20. Systematics of quadrupole and triaxial deformations observed in the ground-state bands of neutron-rich $Z = 39, 41, 43, 45$ isotopes. In the calculations Lund convention was used for γ, which is confined to 0 to -60° (see table 5). The data of ^{111,113}Rh and ^{107}Tc are taken from [17, 18]. A correlation of quadrupole deformations and triaxiality in the Y, Nb, Tc and Rh neutron-rich isotopes can be seen in the figure (see details of discussions in text).

At the same time, it can be seen in figure 20 that the nuclear shape changes from axial symmetry in the case of Y to nearly maximum triaxiality in Rh. With Z increasing, the triaxial deformation increases while quadrupole deformation decreases. Such a correlation of the quadrupole deformation and of triaxiality is generally known. It has been examined in quantitative terms in [34].

5. Summary

New level schemes of ^{99,101}Y and ^{101,105}Nb proposed in the present work provide spectroscopic information about the shape trends and triaxiality in the neutron-rich nuclei with odd-$Z = 39$,

41 in the $A \sim 100$ region. Very small signature splitting is observed in the ground-state bands of $_{39}$Y isotopes, in pronounced contrast to the large ones in $_{43}$Tc and $_{45}$Rh isotopes, the latter being reported to have triaxial deformations [17, 18]. There is a trend of band crossing occurring at higher rotational frequencies in the ground-state bands of Y compared to the Tc and Rh isotopes. This is similar to the observations in the even–even $_{40}$Zr and $_{42}$Mo isotopes, which was accounted for by triaxiality in Mo and axially symmetric shape in Zr isotopes. However, intermediate values of the signature splitting and band crossing frequency between $_{39}$Y and $_{43}$Tc, $_{45}$Rh are observed in $_{41}$Nb isotopes.

Triaxial-rotor-plus-particle model calculations favour a pure axially symmetric shape with large quadrupole deformations for the ground-state bands in Y ($Z = 39$) isotopes. The best fits for the $5/2^+[422]$ ground-state bands in Nb ($Z = 41$) isotopes imply small triaxiality with γ from -13° to -19° while the nearly axially symmetric shape with $\gamma = -5^\circ$ is obtained for the negative-parity bands in the Nb isotopes.

All the above observations and interpretations imply that while large and near maximum of triaxial deformations are identified in $_{43}$Tc and $_{45}$Rh isotopes an axially symmetric and strongly deformed shape is seen in $_{39}$Y isotopes. A correlation of quadrupole deformation and of triaxiality is seen in the nuclei with Z ranging from 39 to 45. The $_{41}$Nb isotopes, having intermediate values of signature splitting and band crossing frequency between Y and Tc, Rh isotopes, are transitional regarding the triaxial degree of freedom. One may conclude that in the $A \sim 100$ neutron-rich nuclei the triaxial shape is prevalent for the bands based on a one-quasiparticle $g_{9/2}$ proton state in the region with $Z > 41$. A shape transition is thus identified from axially symmetric in Y isotopes to triaxiality with large γ values in Tc and Rh isotopes. More detailed information can be useful for further understanding of the transitional Nb nuclei.

Acknowledgments

The works at Vanderbilt University, Lawrence Berkeley National Laboratory, Lawrence Livermore National Laboratory and Idaho National Laboratory are supported by US Department of Energy under grant no. DE-FG05-88ER40407 and contract nos. W-7405-ENG48, DE-AC03-76SF00098 and DE-AC07-99ID13727. The work at Tsinghua University in Beijing is supported by the Major State Basic Research Development Program under contract no. G2000077400 and the Chinese National Natural Science Foundation under grant no. 10375032. The Joint Institute for Heavy Ion Research is supported by its members, University of Tennessee, Vanderbilt and the US DOE. The authors are indebted for the use of ^{252}Cf to the office of Basic Energy Sciences, US Department of Energy, through the transplutonium element production facilities at the Oak Ridge National Laboratory. Dr Augusto Macchiavelli provided valuable help in setting up the Gammasphere electronics for data taking. Dr Ken Gregorich was instrumental in designing the source mounting and plastic absorber ball and in mounting the source. The authors would also like to acknowledge the essential help of I Ahmad, J Greene and R V F Janssens in preparing and lending the ^{252}Cf source they used in the year 2000 runs. The authors greatly appreciate Dr David Radford's developing and providing the new less-compressed Radware cube program.

References

[1] Skalski J, Mizutori S and Nazarewicz W 1997 *Nucl. Phys.* A **617** 282
[2] Hamilton J H 1989 *Treatise on Heavy Ion Science* vol 8 ed Allan Bromley (New York: Plenum) p 2
[3] Cheifetz E *et al* 1970 *Phys. Rev. Lett.* **25** 38

[4] Hamilton J H *et al* 1995 *Prog. Part. Nucl. Phys.* **35** 635
[5] Hamilton J H 1985 *Proc. Int. Symp. on Nuclear Shell Models* ed M Vallieres and B H Wildenthal (Singapore: World Scientific) p 31
Hamilton J H 1985 *Prog. Part. Nucl. Phys.* **15** 107
[6] Becker K *et al* 1984 *Z. Phys.* A **319** 193
[7] Mach H *et al* 1989 *Phys. Lett.* B **230** 21
[8] Hotchkis M A C *et al* 1991 *Nucl. Phys.* A **530** 111
[9] Shizuma K *et al* 1983 *Z. Phys.* A **311** 71
[10] Hua H *et al* 2004 *Phys. Rev.* C **69** 014317
[11] Zell K O *et al* 1984 *Z. Phys.* A **316** 351
[12] Hoellinger F *et al* 1999 *Eur. Phys. J.* A **4** 319
[13] Bauchet A 2001 *Eur. Phys. J.* A **10** 145
[14] Espinoza-Quinones F R 1997 *Phys. Rev.* C **55** 2787
[15] Venkova Ts *et al* 1999 *Eur. Phys. J.* A **6** 405
[16] Venkova Ts *et al* 2002 *Eur. Phys. J.* A **15** 429
[17] Luo Y X *et al* 2004 *Phys. Rev.* C **69** 024315
[18] Luo Y X *et al* 2004 *Phys. Rev.* C **70** 044310
[19] Firestone R B and Shirley V S 1996 *Table of Isotopes* 8th edn (New York: Wiley) and CD ROM 1998 Update
[20] Monnand E *et al* 1982 *Z. Phys.* A **306** 183
[21] Meyer R A *et al* 1985 *Nucl. Phys.* A **439** 510
[22] Petry R F *et al* 1988 *Phys. Rev.* C **37** 2704
[23] Wohn F K *et al* 1985 *Phys. Rev.* C **31** 634
[24] Hwang J K *et al* 1998 *Phys. Rev.* C **58** 3252
[25] Hua H *et al* 2002 *Phys. Rev.* C **65** 064325
[26] Baxter A M *et al* 1992 *Nucl. Instrum. Methods* A **317** 101
[27] Radford D C 1995 *Nucl. Instrum. Methods Phys. Rev.* A **361** 297
Radford D C, Radware, http://radware.phy.ornl.gov/
[28] Luo Y X *et al* 2001 *Phys. Rev.* C **64** 054306
[29] Larsson S E, Leander G and Ragnarsson I 1978 *Nucl. Phys.* A **307** 189
[30] Nilsson S G and Ragnarsson I 1995 *Shapes and Shells in Nuclear Structure* (Cambridge, UK: Cambridge University Press)
[31] Bohr A and Mottelson B 1975 *Nuclear Structure* vol 2 (New York: Benjamin)
[32] Raman S, Nestor C W and Tikkanen P 2001 *At. Nucl. Data* **78** 1
[33] Casten R F 1985 *Nucl. Phys.* A **443** 1
[34] Esser L, Neuneyer U, Casten R F and von Brentano P 1997 *Phys. Rev.* C **55** 206